

Three-dimensional flat bands and possible interlayer triplet pairing superconductivity in the alternating twisted $NbSe_2$ moiré bulk

Shuang Liu(刘爽), Peng Chen(陈鹏), and Shihao Zhang(张世豪)
Citation: Chin. Phys. B, 2026, 35 (**2**): 026801. DOI: 10.1088/1674-1056/ae23ac
http://cpb.iphy.ac.cn; http://iopscience.iop.org/cpb

What follows is a list of articles you may be interested in

Quantum tunneling in the surface diffusion of single hydrogen atoms on Cu(001)

Xiaofan Yu(于小凡), Yangwu Tong(童洋武), and Yong Yang(杨勇)
Chin. Phys. B, 2023, 32 (**8**): 086801. DOI: 10.1088/1674-1056/acd2b4

Reconstruction and stability of Fe_3O_4(001) surface: An investigation based on particle swarm optimization and machine learning

Hongsheng Liu(柳洪盛), Yuanyuan Zhao(赵圆圆), Shi Qiu(邱实), Jijun Zhao(赵纪军), and Junfeng Gao(高峻峰)
Chin. Phys. B, 2023, 32 (**5**): 056802. DOI: 10.1088/1674-1056/acb9e4

Rational design of Fe/Co-based diatomic catalysts for Li-S batteries by first-principles calculations

Xiaoya Zhang(张晓雅), Yingjie Cheng(程莹洁), Chunyu Zhao(赵春宇), Jingwan Gao(高敬莞), Dongxiao Kan(阚东晓), Yizhan Wang(王义展), Duo Qi(齐舵), and Yingjin Wei(魏英进)
Chin. Phys. B, 2023, 32 (**3**): 036803. DOI: 10.1088/1674-1056/aca6da

Realization of semiconducting Cu_2Se by direct selenization of Cu(111)

Yumu Yang(杨雨沐), Qilong Wu(吴奇龙), Jiaqi Deng(邓嘉琦), Jing Wang(王静), Yu Xia(夏雨), Xiaoshuai Fu(富晓帅), Qiwei Tian(田麒玮), Li Zhang(张力), Long-Jing Yin(殷隆晶), Yuan Tian(田园), Sheng-Yi Xie(谢声意), Lijie Zhang(张利杰), and Zhihui Qin(秦志辉)
Chin. Phys. B, 2021, 30 (**11**): 116802. DOI: 10.1088/1674-1056/ac0037

Two-dimensional PC_3 as a promising anode material for potassium-ion batteries: First-principles calculations

Chun Zhou(周淳), Junchao Huang(黄俊超), and Xiangmei Duan(段香梅)
Chin. Phys. B, 2021, 30 (**5**): 056801. DOI: 10.1088/1674-1056/abf10e

---

SPECIAL TOPIC — Moiré physics in two-dimensional materials

Three-dimensional flat bands and possible interlayer triplet pairing superconductivity in the alternating twisted $NbSe_2$ moiré bulk

Shuang Liu(刘爽)[1,2], Peng Chen(陈鹏)[2,3,4], and Shihao Zhang(张世豪)[1,†]

[1] *School of Physics and Electronics, Hunan University, Changsha* 410082, *China*
[2] *Department of Physics, Guangdong Technion – Israel Institute of Technology, Shantou* 515063, *China*
[3] *Department of Physics, Technion – Israel Institute of Technology, Haifa* 32000, *Israel*
[4] *Guangdong Provincial Key Laboratory of Materials and Technologies for Energy Conversion, Guangdong Technion – Israel Institute of Technology, Shantou* 515063, *China*

(Received 20 September 2025; revised manuscript received 13 November 2025; accepted manuscript online 25 November 2025)

Moiré superlattices hosting flat bands and correlated states have become a central focus in condensed matter research. Using first-principles calculations, we investigate three-dimensional flat bands in alternating twisted $NbSe_2$ moiré bulk structures, which exhibit stronger interlayer interactions than twisted bilayer configurations. Our results show that moiré bulks undergo spontaneous large-scale structural relaxation, leading to the formation of remarkably flat energy bands at twist angles $\leq 7.31°$. The k_z-dependent dispersion of these flat bands across different moiré bulks highlights their intrinsic three-dimensional character. Moreover, the presence of out-of-plane mirror symmetry in these moiré bulk structures indicates potential interlayer triplet superconducting pairing mechanisms, distinct from those in twisted bilayer systems. This work opens new avenues for exploring three-dimensional flat bands in other moiré bulk systems.

Keywords: moiré superlattices, first-principles calculations, electronic structure

PACS: 68.65.–k, 71.15.Mb, 73.21.Cd, 74.20.–z

DOI: 10.1088/1674-1056/ae23ac **CSTR:** 32038.14.CPB.ae23ac

1. Introduction

Superconductivity in electronic systems with interacting electrons remains a long-standing and captivating topic in condensed matter physics. Recent breakthroughs in twisted bilayer graphene (TBG) have highlighted the critical role of engineered electronic band structures, particularly flat bands near the Fermi level, in enabling unconventional superconductivity and correlated insulating states.[1–3] These discoveries have propelled the field of twistronics, where controlled rotational misalignment in van der Waals (vdW) structures produces moiré patterns that dramatically modify the electronic structure, creating flat bands. Within such systems, the electron-electron Coulomb interaction dominates over the kinetic energy,[2–7] providing a fertile platform to explore the interplay and competition between superconductivity and electronic correlations.[8–37]

Within twistronics, the transition metal dichalcogenide (TMD) family has attracted significant attention.[38–56] In particular, the three-dimensional spiral structures of TMDs, involving screw dislocations, have been successfully synthesized via chemical vapor deposition (CVD) experiments.[57–60] Theoretical studies have revealed the existence of three-dimensional (3D) flat bands in graphite moiré bulks,[61] suggesting the possibility of novel states in other 3D moiré structures.

Among TMDs, $NbSe_2$ exhibits both superconductivity and charge density waves in few-layer and bulk forms. The superconducting critical temperature increases with the number of layers,[62] indicating that twisted $NbSe_2$ bulks may exhibit higher critical temperatures than twisted few-layer systems. Variations in layer number and twist angle in twisted $NbSe_2$ lead to diverse structural transitions, which influence interlayer coupling and electronic properties. These features make twisted $NbSe_2$ bulks a promising platform for studying 3D flat bands and superconductivity.

In this work, using first-principles methods, we systematically study the evolution of atomic displacements, band structures, and bandwidths for twist angles ranging from 13.17° to 4.41°. The moiré bulk undergoes spontaneous large-scale structural relaxation and exhibits extremely flat energy bands for twist angles not exceeding 7.31°. Furthermore, the flat bands in different moiré structures display k_z-dependent dispersion, indicating the presence of three-dimensional flat bands in alternating twisted $NbSe_2$ moiré bulks. Notably, the bandwidth at 6.00° is narrower than that of 1.05° TBG. Additionally, the out-of-plane mirror symmetry in the moiré bulk leads to a distinct interlayer triplet pairing for superconductivity, distinguishing it from twisted $NbSe_2$ bilayer systems.

†Corresponding author. E-mail: zhangshh@hnu.edu.cn

© 2026 Chinese Physical Society and IOP Publishing Ltd. All rights, including for text and data mining, AI training, and similar technologies, are reserved.

2. Calculation methods

Structural optimizations of twisted $NbSe_2$ bulks were performed using OpenMX with the Perdew–Burke–Ernzerhof (PBE) exchange–correlation functional. Norm-conserving pseudopotentials and pseudo-atomic orbitals Se7.0-s3p2d2 and Nb7.0-s3p2d2 were employed.[63,64] During structural relaxations, a k-points grid of $1\times1\times2$ was used, with a force convergence criterion of 10^{-3} Hartree/Bohr. The DFT-D3 method was applied to account for vdW interactions during structure optimizations.[65]

Band structures at various twist angles were calculated using the real-space electronic structure method implemented in the RESCU package.[66] In self-consistent calculations, a k-points grid of $2\times2\times4$ was used for twist angles from 13.17° to 6.01°, and $1\times1\times4$ for 5.09° and 4.41° twists. The self-consistent procedure was considered converged when the charge variation per valence electron was less than 10^{-6} e. The reliability of RESCU was verified by comparison with VASP[67–70] results for bulk and large-angle twisted $NbSe_2$, as shown in Fig. S1.

3. Results and discussions

3.1. Twisted bulk structures

The crystal structure of a $NbSe_2$ monolayer is illustrated in Fig. 1(a), with each layer lacking inversion symmetry. In this study, we consider moiré bulks consisting of alternating twisted $NbSe_2$ layers, as depicted in Fig. 1(b). In all calculations, the out-of-plane lattice parameter is fixed to the relaxed value of the aligned bilayer, 13.4 Å. In these moiré bulks, only C_{3z} rotational symmetry and M_z mirror symmetry are preserved, while inversion symmetry and M_y mirror symmetry are broken.

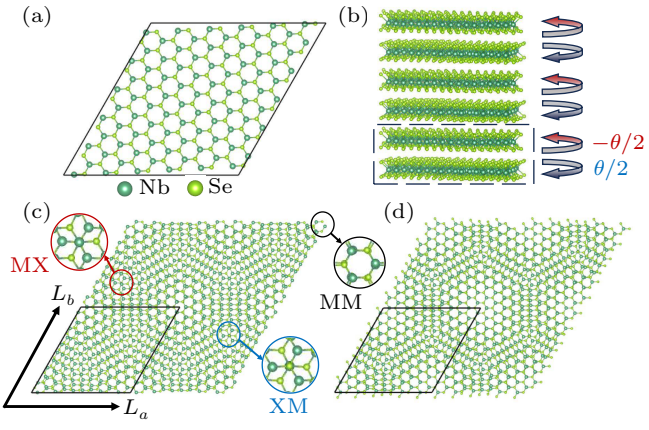


Fig. 1. (a) Top view of monolayer $NbSe_2$. (b) Side view of alternating twisted $NbSe_2$ moiré bulk, with the unit cell indicated by black dashed lines. (c) Unrelaxed structure of the alternating 6.01°-twisted $NbSe_2$ moiré bulk. (d) Relaxed structure of the alternating 6.01°-twisted $NbSe_2$ moiré bulk. Compared to the unrelaxed structure, the relaxed structure exhibits a clear expansion of the MM region.

The lattice vectors of moiré unit cells can be described by a pair of integers (m,n).[71,72] One of the moiré lattice vectors is given by $L_a = ml_a + nl_b$, where l_a and l_b are the lattice vectors of the constituent monolayers. The commensurate twist angle θ is related to (m,n) via

$$\cos\theta = \frac{1}{2}\frac{m^2+n^2+4mn}{m^2+n^2+mn}. \tag{1}$$

The other moiré lattice vector, L_b, is obtained by rotating L_a by 60°. In our study, the twist angle θ ranges from 4.41° to 13.17°. The relationship between twist angle, number of atoms, and integers (m,n) in the moiré unit cell is summarized in Table 1.

Figure 1(c) shows the unrelaxed 6.01°-twisted moiré pattern of $NbSe_2$ bulk from the top view. Three high-symmetry stacking configurations exist within the moiré unit cell, namely MM, MX, and XM. The center of the MM region coincides with the origin, while the centers of the MX and XM regions are located at $(L_a+L_b)/3$ and $2(L_a+L_b)/3$, respectively. The relaxed structure is shown in Fig. 1(d), where the MM region is significantly expanded compared to the unrelaxed case, and the MX and XM regions are reduced to narrow domain walls.

Table 1. Relationship between twist angle, number of atoms N_{atoms}, and integers (m,n) in the moiré unit cell.

n	m	Angle	N_{atoms}
2	3	13.17°	114
3	4	9.43°	222
4	5	7.34°	366
5	6	6.01°	546
6	7	5.09°	762
7	8	4.41°	1014

In the relaxed structure, the atomic displacements for $\theta = 13.17°$ and $\theta = 4.41°$ are shown in Fig. 2. In the large-angle ($\theta = 13.17°$) twisted structure, only a few atoms exhibit significant displacements. In the top layer, displacements around the MX site occur in a clockwise direction, while in the bottom layer, displacements around the XM site are counterclockwise. By contrast, in the small-angle twisted structure ($\theta = 4.41°$), distinctive vortex-like displacement patterns emerge, predominantly around the MM site, resulting in an enlarged MM region within the moiré structure. Each layer experiences interlayer interactions from both adjacent layers, which collectively suppress large out-of-plane corrugations in the moiré bulk structure. These displacement patterns are consistent with Ref. [73] and reveal pronounced vortex-like spontaneous atomic rearrangements in the moiré bulk. The large-angle twisted bulk $NbSe_2$ system ($\theta \leq 7.34°$) exhibits significant atomic relaxation, which in bilayer $NbSe_2$ occurs only at small angles ($\theta \leq 3.14°$).[73] This highlights a key finding of our work: twisted bulk $NbSe_2$ enables enhanced atomic relaxation through strong interlayer interactions.

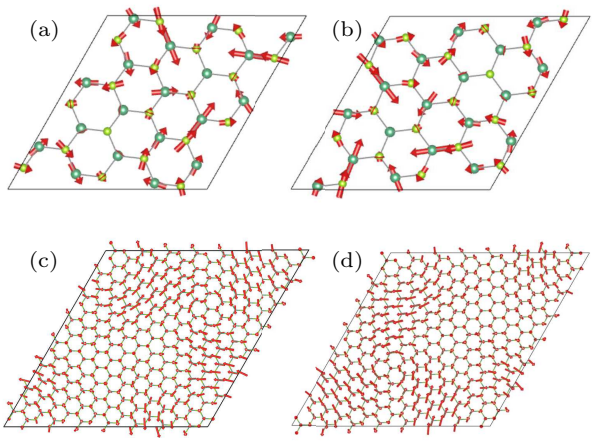


Fig. 2. Atomic displacements in the top layer (a) and bottom layer (b) of the unit cell in the alternating 13.17°-twisted $NbSe_2$ moiré bulk are shown. The length of the red vectors on each atom represents the displacement amplitude, with a scaling factor of 25. Atomic displacements in the top layer (c) and bottom layer (d) of the alternating 4.41°-twisted $NbSe_2$ moiré bulk are also shown, with a scaling factor of 3. See Fig. S2 for clearer displacement distributions.

3.2. Electronic properties

To investigate the three-dimensional electronic structure of twisted $NbSe_2$ bulk, we calculated the band structures on different k_x–k_y planes across the Brillouin zone ($k_z = 0$, $\pi/3$, $\pi/2$). As shown in Fig. 3, the energy bands near the Fermi level exhibit clear k_z-dependence in the alternating twisted $NbSe_2$ moiré bulk.

In the unrelaxed structure of alternating twisted $NbSe_2$ moiré bulks with $\theta = 13.17°$, 9.43°, 7.32°, and 6.01°, hole pockets appear at the Γ point. In the relaxed structure, however, hole pockets persist only for the $\theta = 13.17°$ and 9.43° twist angles. This change arises because the energy bands become increasingly dispersionless in the relaxed structures with smaller twist angles. Notably, the large bandgaps at the Γ point vanish after relaxation, and additional electronic states emerge near the Fermi level for $\theta \leq 7.34°$.

These results indicate that spontaneous structural relaxation in the alternating twisted $NbSe_2$ moiré bulk plays a crucial role in shaping the electronic structure. The expansion of MM stacking regions and the contraction of MX/XM domains into narrow domain walls localize the electronic states in real space, which further suppresses the kinetic energy and leads to flatter energy bands.

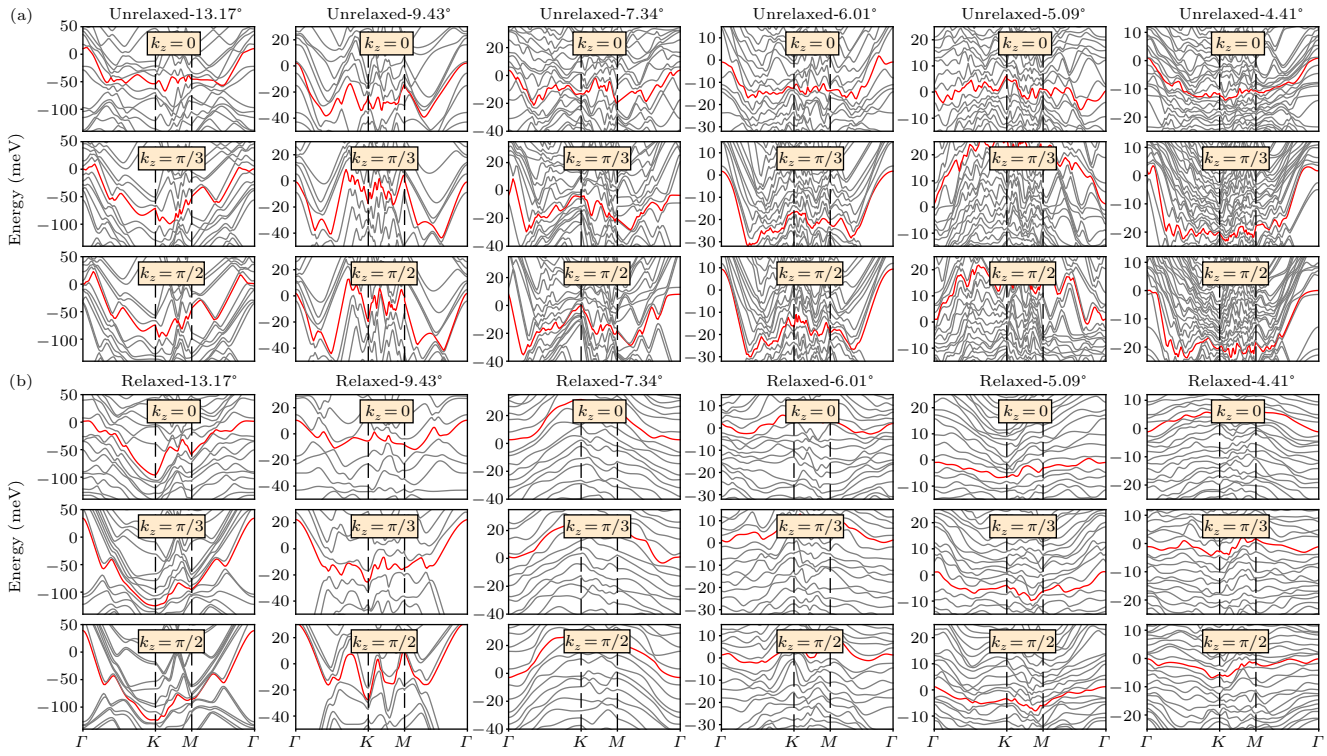


Fig. 3. Energy bands of the alternating twisted $NbSe_2$ moiré bulk for both unrelaxed and relaxed structures. The bands closest to the Fermi level are highlighted.

We note that lattice relaxation in twisted bilayer graphene leads to gap opening at ±4 filling and induces particle–hole asymmetry.[74–77] In contrast, the twisted $NbSe_2$ bulk exhibits a dense set of mini-bands near the Fermi level, originating from the conducting bands within the primitive unit cell of the $NbSe_2$ monolayer. Atomic relaxation does not produce similarly isolated flat bands in twisted $NbSe_2$ bulk, which can be attributed to strong intralayer hopping and the relatively large intrinsic bandwidth of $NbSe_2$ compared to the interlayer interaction.

In the $NbSe_2$ monolayer, the energy bands at the Γ valley primarily arise from d_{z^2} orbitals, whereas in the K valley, they

are mainly contributed by $d_{xy}+d_{x^2-y^2}$ orbitals.[78] Orbital-projection analysis for the 21.79° twisted bulk (Fig. S4) confirms that the flat bands near the Fermi energy exhibit K-valley character and are dominated by the $d_{xy}+d_{x^2-y^2}$ orbitals.

Two distinct stacking configurations exist in twisted TMDs, centered on either the MM or MX region.[79] In the MX-stacking twisted TMD, one layer is obtained by rotating by 180° around the hollow site relative to the MM-stacking configuration. Previous work[79] showed that the electronic structures differ significantly between these two stacking types. Accordingly, we also calculated the electronic structure of 13.17° and 6.01° twisted bulk with AP-centered (MX-centered) stacking, as shown in Fig. 4.

Although the overall band shapes differ between the MX- and MM-centered twisting structures, the bandwidths of bands near the Fermi energy remain similar: 93.3 meV (MX) vs. 102.3 meV (MM) for 13.17°, and 12.6 meV (MX) vs. 11.1 meV (MM) for 6.01°. These results indicate that the bandwidths of bands near the Fermi energy are largely insensitive to the stacking center.

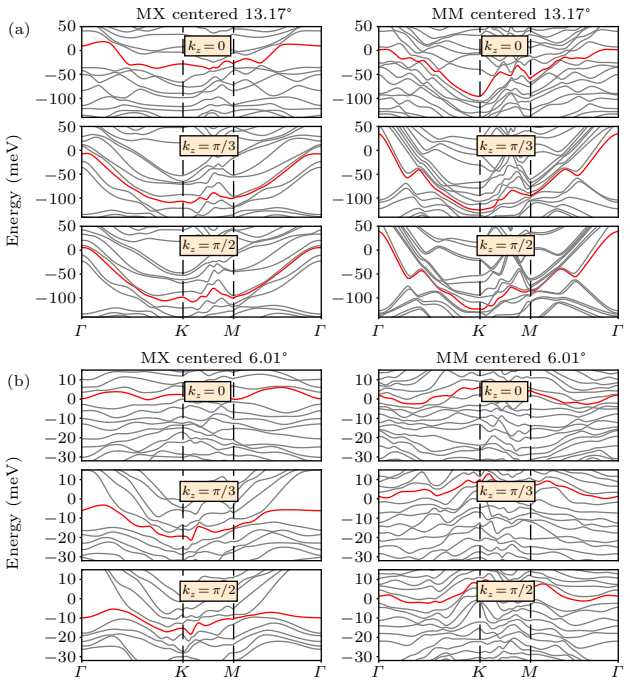


Fig. 4. Band structures of twisted $NbSe_2$ at 13.17° and 6.01° with MX- and MM-centered rotation, respectively (results from the main text).

To trace the evolution of the bandwidth with decreasing twist angle, we focus on the bands closest to the Fermi level. The average bandwidth of these bands at different k_z values is used as an indicator of the system's overall bandwidth. As shown in Fig. 5, the bandwidth of the alternating 7.34°-twisted $NbSe_2$ moiré bulk decreases to 30 meV. In the alternating 6.01°-twisted $NbSe_2$ moiré bulk, the bandwidth is further reduced to 10 meV, comparable to the typical bandwidths of magic-angle twisted bilayer graphene (Fig. 5).

These results indicate that three-dimensional flat bands emerge in alternating twisted $NbSe_2$ moiré bulk for twist angles $\theta \leq 6.01°$, where strong electron–electron interactions can occur. As also shown in Fig. 5, atomic relaxation in the twisted moiré bulk enhances the density of states (DOS) near the Fermi level. The small bandwidth of the mini-bands induced by atomic relaxation produces a series of sharp DOS peaks in the 6.01°, 5.09°, and 4.41° twisted $NbSe_2$ bulk.

In the alternating twisted $NbSe_2$ moiré bulk, each layer experiences interlayer interactions from two neighboring layers. In contrast, in twisted bilayer $NbSe_2$ or at the surface of the moiré bulk, these interlayer interactions are weaker, leading to broader moiré bands. Consequently, the surface states behave differently from the bulk states in the alternating twisted $NbSe_2$ moiré bulk.

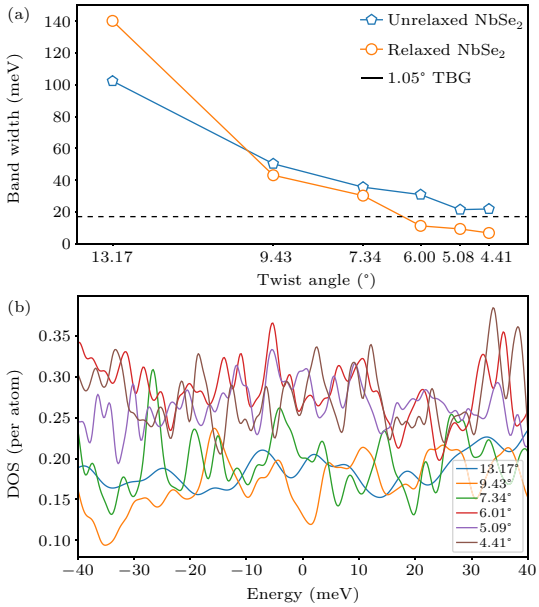


Fig. 5. (a) Average bandwidths of the energy bands highlighted in Fig. 3 for different alternating twisted $NbSe_2$ moiré bulks. (b) Calculated DOS per atom for different twisted $NbSe_2$ bulks.

3.3. Electron Coulomb interaction

The electron Coulomb interaction can be expressed as

$$H = V(q)c^{\dagger}_{k+q}c^{\dagger}_{k'-q}c_{k'}c_{k}, \tag{2}$$

where k, k', q are wave vectors in the Brillouin zone. In 2D systems, the screened Coulomb interaction is given by

$$V(q) = \frac{e^2}{2\Omega_M \varepsilon \varepsilon_0 \sqrt{q^2+\kappa^2}}, \tag{3}$$

where Ω_M is the moiré lattice area, κ is the inverse screening length, and ε is the background dielectric constant. In 3D systems, the interaction becomes

$$V(q) = \frac{e^2}{d\,\Omega_M \varepsilon \varepsilon_0 (q^2+\kappa^2)}, \tag{4}$$

where d is the out-of-plane lattice constant. Experimentally, κ ranges from 0.002 $Å^{-1}$ to 0.02 $Å^{-1}$. For small q (satisfying

$d\sqrt{q^2+\kappa^2} < 2$), the 3D electron interaction is stronger than that in 2D systems.

In the 6.01° twisted $NbSe_2$ moiré bulk, for $q \sim 0.1G = 0.022$ Å^{-1} (G is the in-plane reciprocal lattice vector) and $\kappa = 0.01$ Å^{-1}, we find

$$\frac{2}{d\sqrt{q^2+\kappa^2}} \approx 6.176,$$

indicating that the 3D electron Coulomb interaction is roughly six times stronger than in the 2D case. The 3D Coulomb interaction decays rapidly as $1/q^2$, and $V(q=0.1G)/V(q=0.316G) \approx 10$ demonstrates its short-range nature. Thus, in the 3D moiré bulk, the dominant electron interactions originate from small-q scattering.

In contrast, in quasi-2D twisted bilayer systems, the 2D Coulomb interaction decays more slowly as $1/q$, and interband scattering cannot be neglected, which hinders the realization of correlated states. In the twisted moiré bulk, despite the presence of multiple bands near the Fermi level, the rapid $1/q^2$ decay confines the dominant electron interactions to a few low-energy bands. This feature effectively relaxes the requirement of isolated flat bands that is necessary in 2D twisted systems.

In alternating twisted trilayer graphene, flat bands coexist with highly dispersive Dirac cones near the Fermi level.[80,81] Nevertheless, correlated states have been experimentally observed, and theoretical studies[82] describe these as intervalley coherent states. This demonstrates that overlapping bands do not necessarily suppress correlated states, suggesting that multi-band scattering may not preclude correlated states in alternating twisted $NbSe_2$ bulk.

As the twist angle decreases, the moiré supercell enlarges, and band folding further reduces the bandwidth. We define the characteristic interaction energy on the moiré length as[23]

$$U_M = \frac{e^2}{4\pi\varepsilon\varepsilon_0 L_S}. \tag{5}$$

For comparison, in magic-angle twisted bilayer graphene, $U_M \approx 22$ meV, exceeding the flat-band bandwidth. In the 6.01° twisted $NbSe_2$ moiré bulk, the reciprocal lattice length is four times larger, yielding $U_M \approx 88$ meV, much larger than the bandwidths. These estimates place the 6.01° twisted $NbSe_2$ moiré bulk firmly in the strong-interaction regime favorable for correlated electron physics.

3.4. Interlayer triplet pairing superconductivity

$NbSe_2$ exhibits superconductivity in few-layer and bulk forms. Here, we discuss possible superconductivity in the alternating twisted $NbSe_2$ moiré bulk. In superconducting materials, the electrodynamic response is described by

$$\boldsymbol{j} = -D_s \boldsymbol{A}, \tag{6}$$

where $\boldsymbol{j}$ is the current density, $\boldsymbol{A}$ is the vector potential, and D_s is the superfluid weight. The superfluid weight, a key criterion for superconductivity, can be decomposed into a conventional contribution and a geometric contribution.[10] The conventional contribution arises from single-band effects, whereas the geometric contribution originates from multi-band effects. In flat-band systems, the geometric superfluid weight dominates. Therefore, in alternating twisted $NbSe_2$ bulk with small twist angles, the geometric superfluid weight plays a particularly significant role.

Although increased effective mass enhances band flatness, the geometric superfluid weight also depends sensitively on the wavefunction geometry.[83] The role of wavefunction geometry in superconductivity in the alternating twisted $NbSe_2$ bulk warrants further study.

The continuum Hamiltonian for the superconducting pairing can be written as

$$H_{sc}(\boldsymbol{r}) = \int \mathrm{d}\boldsymbol{r} \sum_{\xi ll' ss'} \psi^\dagger_{\xi ls}(\boldsymbol{r}) \Delta_{ll',ss'}(\boldsymbol{r}) \psi^\dagger_{-\xi l's'}(\boldsymbol{r}) + \text{h.c.}, \tag{7}$$

where ξ denotes the valley index, and l or l' labels the layer in the moiré bulk unit cell. Following previous studies,[84,85] we consider only momentum-direction-independent pairing for simplicity. Since the electronic band structure reflects only single-particle wavefunctions, symmetry constraints must be applied to determine the allowed form of the pairing.

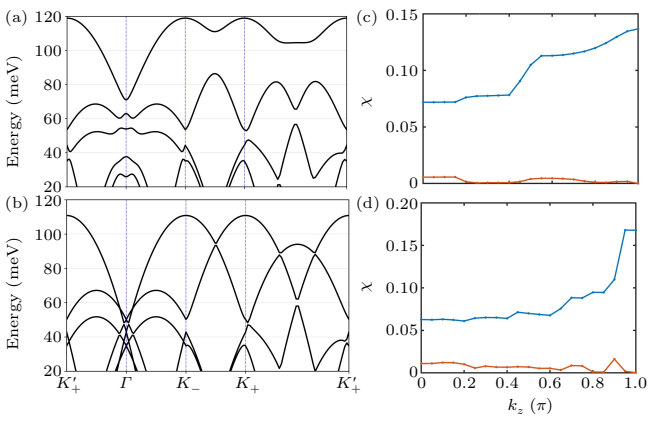


Fig. 6. Energy bands of the effective model at a 5° twist angle in the (a) $k_z = 0$ and (b) $k_z = \pi$ planes. The calculated k_z-resolved pairing susceptibility at chemical potentials of (c) $\mu = 50$ meV and (d) $\mu = 80$ meV. Blue lines correspond to the k_z-resolved pairing susceptibility in the $\gamma_{y0} = \tau_y$ channel, while red lines represent the susceptibility of a mixture between the $\gamma_{y0} = \tau_y$ and $\gamma_{yz} = \tau_y s_z$ channels.

To begin, we analyze the possible superconducting pairings in twisted bilayer $NbSe_2$. The system exhibits $\mathcal{T} \times D_3$ symmetry.[85] Accordingly, twisted bilayer $NbSe_2$ has time-reversal symmetry $\mathcal{T} = \mathrm{i}s_y\mathcal{K}$, three-fold rotational symmetry $C_{3z} = \mathrm{e}^{\mathrm{i}2\pi s_z/3}$, and two-fold rotational symmetry $C_{2y} = -\mathrm{i}\tau_x s_y$, where τ and s are Pauli matrices defined in layer and spin space, respectively.

There are six matrices of pairing wavefunctions that can couple to s-wave pairings: s_y, $\tau_x s_y$, $\tau_z s_y$, τ_y, $\tau_y s_x$, and

$\tau_y s_z$. Among these, only the set $\{\tau_y, \tau_y s_z\}$ belongs to a two-dimensional irreducible representation, while the others belong to one-dimensional irreducible representations. Specifically, $(\tau_0, \tau_x)s_y$, $\tau_z s_y$, and $\tau_y s_x$ describe singlet pairings, whereas $\{\tau_y, \tau_y s_z\}$ corresponds to triplet pairing.

In the alternating twisted $NbSe_2$ bulk, the additional mirror symmetry $M_z = \mathrm{i}s_z$ forbids all pairings belonging to one-dimensional irreducible representations. Consequently, only the triplet pairing $\{\tau_y, \tau_y s_z\}$ is allowed, with the explicit BCS form

$$\begin{aligned}\Psi_{\mathrm{BCS}} = &\{\psi_{-\xi-\boldsymbol{k},l\uparrow}\psi_{\xi+\boldsymbol{k},l'\uparrow} + \psi_{-\xi-\boldsymbol{k},l\downarrow}\psi_{\xi+\boldsymbol{k},l'\downarrow},\\ &\psi_{-\xi-\boldsymbol{k},l\uparrow}\psi_{\xi+\boldsymbol{k},l'\uparrow} - \psi_{-\xi-\boldsymbol{k},l\downarrow}\psi_{\xi+\boldsymbol{k},l'\downarrow}\},\\ &(l \neq l').\end{aligned} \tag{8}$$

Thus, only interlayer triplet pairing can exist in the alternating twisted $NbSe_2$ bulk, distinguishing it from the twisted bilayer system.

Now we turn to the microscopic model of superconductivity in the twisted moiré bulk. We start with the $NbSe_2$ monolayer, which hosts conducting bands crossing the Fermi level. Its electronic structure differs from those of insulating MoS_2 and $MoTe_2$ monolayers. While the continuum models of twisted MoS_2 and $MoTe_2$ can be accurately described by states near the K valley, an accurate continuum model of twisted $NbSe_2$ requires the full Hamiltonian across the entire Brillouin zone. To construct a minimal model for superconductivity in the twisted moiré bulk, we note that the electronic states near the Fermi level originate predominantly from the K valley. Thus, we adopt the following continuum Hamiltonian:

$$H_\xi(\boldsymbol{r}) = \begin{pmatrix} h_{\mathrm{b}}(\boldsymbol{r}) & \hat{T}(\boldsymbol{r})(1+\mathrm{e}^{\mathrm{i}k_z}) \\ \hat{T}^\dagger(\boldsymbol{r})(1+\mathrm{e}^{-\mathrm{i}k_z}) & h_{\mathrm{t}}(\boldsymbol{r}) \end{pmatrix}, \tag{9}$$

where h_{b} and h_{t} are the effective monolayer Hamiltonians near the ξK valley, $\hat{T}$ denotes the interlayer tunneling term, and $\mathrm{e}^{\mathrm{i}k_z}$ accounts for interlayer coupling between neighboring unit cells in the twisted bulk. The detailed parameters of this effective model follow Refs. [54,85]. Our calculated energy bands exhibit k_z-dependent electronic structure, as shown in Figs. 6(a) and 6(b).

We consider interlayer triplet pairing channels represented by the matrices $\gamma_{y0} = \tau_y$ and $\gamma_{yz} = \tau_y s_z$. The pairing susceptibility for a finite-momentum Cooper pair ($\boldsymbol{q} \neq 0$) is defined as

$$\chi_{ij,\mu\nu}(\boldsymbol{q}) = \int_{\boldsymbol{p}} \sum_{a,b} O^{j\nu}_{a,b}(\boldsymbol{p},\boldsymbol{q})\, O^{i\mu *}_{a,b}(\boldsymbol{p},\boldsymbol{q})\, \mathcal{K}_{ab}(\boldsymbol{p},\boldsymbol{q}), \tag{10}$$

where $\boldsymbol{p}$ and $-\boldsymbol{p}$ are the momenta of the electron and hole in the Cooper pair, respectively. The overlap function is

$$O^{j\nu}_{a,b}(\boldsymbol{p},\boldsymbol{q}) = \langle u_{a\boldsymbol{p}+\boldsymbol{q}/2}|\gamma_{j\nu}|v_{b-\boldsymbol{p}+\boldsymbol{q}/2}\rangle, \tag{11}$$

with a and b labeling the bands, and $|u\rangle$ and $|v\rangle$ being the electron and hole eigenstates, respectively. The kernel function is

$$\mathcal{K}_{ab}(\boldsymbol{p},\boldsymbol{q}) = \frac{1 - f(E_a(\boldsymbol{p}+\boldsymbol{q}/2)) - f(E'_b(-\boldsymbol{p}+\boldsymbol{q}/2))}{E_a(\boldsymbol{p}+\boldsymbol{q}/2) + E'_b(-\boldsymbol{p}+\boldsymbol{q}/2)}, \tag{12}$$

where f is the Fermi distribution function and E_a, E'_b are the electron and hole eigenvalues, respectively. In this work, we focus on zero-momentum Cooper pairing ($\boldsymbol{q} = 0$). The corresponding k_z-resolved pairing susceptibility is then

$$\begin{aligned}\chi^{k_z}_{ij,\mu\nu}\quad (\boldsymbol{q}=0) = &\int_{k_x k_y} \sum_{a,b} O^{j\nu}_{a,b}(k_x,k_y,k_z,\boldsymbol{q}=0)\\ &\times O^{i\mu *}_{a,b}(k_x,k_y,k_z,\boldsymbol{q}=0)\,\mathcal{K}_{ab}(k_x,k_y,k_z,\boldsymbol{q}=0).\end{aligned} \tag{13}$$

The calculated $\chi^{k_z}_{ij,\mu\nu}$ at different chemical potentials are shown in Figs. 6(c) and 6(d). These results demonstrate that the non-zero k_z components contribute significantly larger pairing susceptibility compared to the $k_z = 0$ plane, highlighting the crucial role of interlayer coupling in enhancing the triplet pairing in the twisted moiré bulk.

3.5. Further discussions on triplet pairing superconductivity

Extensive research has been devoted to the three-dimensional spiral structures of TMDs associated with screw dislocations. These structures have been successfully realized through chemical vapor deposition (CVD) experiments. Consequently, the alternating twisted bulk TMD may be synthesized using similar experimental techniques.

The minimal structural platform exhibiting the crucial mirror symmetry discussed here is the alternating twisted trilayer system. For example, alternating twisted trilayer graphene has been proposed as a promising platform for realizing spin-triplet superconductivity, largely due to its mirror symmetry.[86] Similarly, an alternating twisted trilayer $NbSe_2$ would also retain mirror symmetry and could potentially support triplet pairing. However, a significant experimental consideration is that such trilayer systems are inherently sensitive to substrate effects, which often break the mirror symmetry. In contrast, the bulk nature of the alternating twisted moiré system studied here provides intrinsic protection of the bulk states against such symmetry-breaking substrate potentials, offering a more robust environment for realizing symmetry-protected phenomena.

We now discuss key spectroscopic and transport probes that can provide characteristic signatures of interlayer triplet pairing.

(i) Scanning tunneling microscopy/spectroscopy (STM/STS) directly measures the local density of states, providing real-space information on the superconducting gap.

(ii) Nuclear magnetic resonance (NMR) can distinguish triplet from singlet pairing. In conventional spin-singlet superconductors, the spin susceptibility decreases below the critical temperature T_c, resulting in a drop in the Knight shift and a Hebel–Slichter peak in the spin-lattice relaxation rate just below T_c, followed by an exponential decay at lower temperatures. In contrast, for spin-triplet pairing, the Knight shift remains unchanged below T_c under an applied magnetic field, since spin polarization is preserved within the Cooper pairs. Additionally, the spin-lattice relaxation rate lacks a Hebel–Slichter peak and exhibits power-law behavior at low temperatures.

(iii) Josephson junction measurements — either vertical junctions with the moiré bulk sandwiched between conventional s-wave superconductors (e.g., Nb) or planar geometries — can provide further insights. The critical current in such junctions is sensitive to the phase and symmetry of the superconducting order parameter. A hallmark of triplet pairing is the potential for a Josephson current that depends distinctly on the orientation of an in-plane magnetic field. Phase-sensitive measurements, such as those employing SQUID interferometers, could in principle detect an anomalous phase shift if the order parameter has an odd-parity component.

Probing the bulk superconducting gap requires more bulk-sensitive techniques, such as soft x-ray ARPES or hard x-ray photoemission spectroscopy (HAXPES). Transport measurements can also reveal triplet superconductivity, as the bulk signal dominates over surface contributions. Surface-parallel channels may broaden the resistive transition or leave a residual resistance, but the emergence of a zero-resistance state remains a definitive indicator of bulk superconductivity. To disentangle surface and bulk contributions, standard van der Pauw measurements on samples of varying thickness can be employed; the bulk-dominated signal should saturate beyond a certain thickness.

The parent compound $NbSe_2$ exhibits charge density wave (CDW) order due to electron–phonon interactions. In the CDW state, time-reversal, C_{3z}, C_{2y}, and mirror symmetries are preserved, which supports the interlayer triplet superconductivity in twisted bulk $NbSe_2$ with CDW order. Nevertheless, the CDW may affect the superconducting transition temperature, and the interplay between CDW and interlayer triplet pairing remains a topic for future theoretical and experimental exploration.

Finally, we note that the discussion above considers only the non-interacting pairing mechanism. In twisted bulk $NbSe_2$, electron correlations can stabilize distinct correlated states. For example, a valley-polarized state that breaks time-reversal symmetry or a nematic state that breaks C_{3z} symmetry removes the constraints on one-dimensional irreducible pairings. Consequently, electron interactions may induce a mixture of interlayer triplet and other pairing channels, while dressed electron-phonon interactions further influence the robustness of the superconducting phase against competing charge orders.

4. Conclusion

In summary, we have investigated three-dimensional flat bands in the alternating twisted $NbSe_2$ moiré bulk using first-principles calculations. In contrast to twisted bilayer systems, each layer in the moiré bulk experiences stronger interlayer interactions. Our results reveal that the moiré bulk undergoes spontaneous large-scale structural relaxation and exhibits remarkably flat energy bands when the twist angle is below 7.31°. The flat bands in these moiré bulks exhibit pronounced k_z-dependence, confirming the existence of three-dimensional flat bands in the alternating twisted $NbSe_2$ moiré bulk. Furthermore, the out-of-plane mirror symmetry of the moiré bulk enables a unique interlayer triplet pairing, distinguishing its superconducting behavior from that of twisted bilayer systems.

Acknowledgments

This work was supported by the National Key Research and Development Program of China (Grant No. 2024YFA1410300), the National Natural Science Foundation of China (Grant No. 12304217), the Natural Science Foundation of Hunan Province (Grant No. 2025JJ60002), and the Fundamental Research Funds for the Central Universities of China (Grant No. 531119200247). We gratefully acknowledge HZWTECH for providing computational facilities.

References

[1] Aoki H 2020 *J. Supercond. Nov. Magn.* **33** 2341
[2] Cao Y, Fatemi V, Fang S, Watanabe K, Taniguchi T, Kaxiras E and Jarillo-Herrero P 2018 *Nature* **556** 43
[3] Cao Y, Fatemi V, Demir A, Fang S, Tomarken S L, Luo J Y, Sanchez-Yamagishi J D, Watanabe K, Taniguchi T, Kaxiras E, Ashoori R C and Jarillo-Herrero P 2018 *Nature* **556** 80
[4] Tang Y, Li L, Li T, Xu Y, Liu S, Barmak K, Watanabe K, Taniguchi T, MacDonald A H, Shan J and Mak K F 2020 *Nature* **579** 353
[5] Regan E C, Wang D, Jin C, Bakti Utama M I, Gao B, Wei X, Zhao S, Zhao W, Zhang Z, Yumigeta K, Blei M, Carlström J D, Watanabe K, Taniguchi T, Tongay S, Crommie M, Zettl A and Wang F 2020 *Nature* **579** 359
[6] Wang L, Shih E M, Ghiotto A, Xian L, Rhodes D A, Tan C, Claassen M, Kennes D M, Bai Y, Kim B, Watanabe K, Taniguchi T, Zhu X, Hone J, Rubio A, Pasupathy A N and Dean C R 2020 *Nat. Mater.* **19** 861
[7] Pasquale G, Sun Z, Čerņevičs K, Perea-Causin R, Tagarelli F, Watanabe K, Taniguchi T, Malic E, Yazyev O V and Kis A 2022 *Nano Lett.* **22** 8883
[8] Wilhelm P, Lang T C and Läuchli A M 2021 *Phys. Rev. B* **103** 205146
[9] Zhang Y, Tan Y W, Stormer H L and Kim P 2005 *Nature* **438** 201
[10] Törmä P, Peotta S and Bernevig B A 2022 *Nat. Rev. Phys.* **4** 528
[11] Lee J Y, Khalaf E, Liu S, Liu X, Hao Z, Kim P and Vishwanath A 2019 *Nat. Commun.* **10** 5333
[12] Wu F, MacDonald A H and Martin I 2018 *Phys. Rev. Lett.* **121** 257001
[13] Codecido E, Wang Q, Koester R, Che S, Tian H, Lv R, Tran S, Watanabe K, Taniguchi T, Zhang F, Bockrath M and Lau C N 2019 *Sci. Adv.* **5** eaaw9770

[14] Lu X, Stepanov P, Yang W, Xie M, Aamir M A, Das I, Urgell C, Watanabe K, Taniguchi T, Zhang G, Bachtold A, MacDonald A H and Efetov D K 2019 *Nature* **574** 653
[15] Stepanov P, Das I, Lu X, Fahimniya A, Watanabe K, Taniguchi T, Koppens F H L, Lischner J, Levitov L and Efetov D K 2020 *Nature* **583** 375
[16] Saito Y, Ge J, Watanabe K, Taniguchi T and Young A F 2020 *Nat. Phys.* **16** 926
[17] Liu X, Wang Z, Watanabe K, Taniguchi T, Vafek O and Li J 2021 *Science* **371** 1261
[18] Cao Y, Rodan-Legrain D, Park J M, Yuan N F, Watanabe K, Taniguchi T, Fernandes R M, Fu L and Jarillo-Herrero P 2021 *Science* **372** 264
[19] Kang J and Vafek O 2019 *Phys. Rev. Lett.* **122** 246401
[20] Seo K, Kotov V N and Uchoa B 2019 *Phys. Rev. Lett.* **122** 246402
[21] Xie M and MacDonald A H 2020 *Phys. Rev. Lett.* **124** 097601
[22] Bultinck N, Chatterjee S and Zaletel M P 2020 *Phys. Rev. Lett.* **124** 166601
[23] Zhang S, Dai X and Liu J 2022 *Phys. Rev. Lett.* **128** 026403
[24] Zhang S, Lu X and Liu J 2022 *Phys. Rev. Lett.* **128** 247402
[25] Bultinck N, Khalaf E, Liu S, Chatterjee S, Vishwanath A and Zaletel M P 2020 *Phys. Rev. X* **10** 031034
[26] Liu J and Dai X 2021 *Phys. Rev. B* **103** 035427
[27] Zhang Y, Jiang K, Wang Z and Zhang F 2020 *Phys. Rev. B* **102** 035136
[28] Hejazi K, Chen X and Balents L 2021 *Phys. Rev. Res.* **3** 013242
[29] Kang J and Vafek O 2020 *Phys. Rev. B* **102** 035161
[30] Chen B B, Liao Y D, Chen Z, Vafek O, Kang J, Li W and Meng Z Y 2021 *Nat. Commun.* **12** 5480
[31] Da Liao Y, Kang J, Breiø C N, Xu X Y, Wu H Q, Andersen B M, Fernandes R M and Meng Z Y 2021 *Phys. Rev. X* **11** 011014
[32] Bernevig B A, Song Z D, Regnault N and Lian B 2021 *Phys. Rev. B* **103** 205413
[33] Lian B, Song Z D, Regnault N, Efetov D K, Yazdani A and Bernevig B A 2021 *Phys. Rev. B* **103** 205414
[34] Xie F, Cowsik A, Song Z D, Lian B, Bernevig B A and Regnault N 2021 *Phys. Rev. B* **103** 205416
[35] Soejima T, Parker D E, Bultinck N, Hauschild J and Zaletel M P 2020 *Phys. Rev. B* **102** 205111
[36] Zhang X, Pan G, Zhang Y, Kang J and Meng Z Y 2021 *Chin. Phys. Lett.* **38** 077305
[37] Parker D E, Soejima T, Hauschild J, Zaletel M P and Bultinck N 2021 *Phys. Rev. Lett.* **127** 027601
[38] Xu C, Li J, Xu Y, Bi Z and Zhang Y 2024 *Proc. Natl. Acad. Sci. USA* **121** e2316749121
[39] Mao N, Xu C, Li J, Bao T, Liu P, Xu Y, Felser C, Fu L and Zhang Y 2024 *Commun. Phys.* **7** 262
[40] Zhang Y, Liu T and Fu L 2021 *Phys. Rev. B* **103** 155142
[41] Xu C, Mao N, Zeng T and Zhang Y 2025 *Phys. Rev. Lett.* **134** 066601
[42] Xu F, Sun Z, Jia T, Liu C, Xu C, Li C, Gu Y, Watanabe K, Taniguchi T, Tong B, Jia J, Shi Z, Jiang S, Zhang Y, Liu X and Li T 2023 *Phys. Rev. X* **13** 031037
[43] Fan F R, Xiao C and Yao W 2024 *Phys. Rev. B* **109** L041403
[44] Tong Q, Yu H, Zhu Q, Wang Y, Xu X and Yao W 2017 *Nat. Phys.* **13** 356
[45] Reddy A P, Devakul T and Fu L 2023 *Phys. Rev. Lett.* **131** 246501
[46] Sheng D N, Reddy A P, Abouelkomsan A, Bergholtz E J and Fu L 2024 *Phys. Rev. Lett.* **133** 066601
[47] Xu F, Chang X, Xiao J, Zhang Y, Liu F, Sun Z, Mao N, Peshcherenko N, Li J, Watanabe K, Taniguchi T, Yang H, Zhou B, Yang L, Zhang Y, Tong W Y and Liu X 2025 *Nat. Phys.* **21** 542
[48] Zhang X W, Wang C, Liu X, Fan Y, Cao T and Xiao D 2024 *Nat. Commun.* **15** 4223
[49] Reddy A P, Alsallom F, Zhang Y, Devakul T and Fu L 2023 *Phys. Rev. B* **108** 085117
[50] Xie Y M, Zhang C P, Hu J X, Mak K F and Law K T 2022 *Phys. Rev. Lett.* **128** 026402
[51] Pan H, Xie M, Wu F and Das Sarma S 2022 *Phys. Rev. Lett.* **129** 056804
[52] Li B and Wu F 2025 *Phys. Rev. B* **111** 125122
[53] Qiu W X, Li B, Luo X J and Wu F 2023 *Phys. Rev. X* **13** 041026
[54] Wu F, Lovorn T, Tutuc E, Martin I and MacDonald A H 2019 *Phys. Rev. Lett.* **122** 086402
[55] Li B, Qiu W X and Wu F 2024 *Phys. Rev. B* **109** L041106
[56] Cai J, Anderson E, Wang C, Zhang X, Liu X, Holtzmann W, Zhang Y, Fan F, Taniguchi T, Watanabe K, Yazdani A, Xu C, Zhang Y and Li T 2023 *Nature* **622** 63
[57] Zhang L, Liu K, Wong A B, Kim J, Hong X, Liu C, Cao T, Louie S G, Wang F and Yang P 2014 *Nano Lett.* **14** 6418
[58] Ci P, Zhao Y, Sun M, Rho Y, Chen Y, Grigoropoulos C P, Jin S, Li X and Wu J 2022 *Nano Lett.* **22** 9027
[59] Fan X, Jiang Y, Zhuang X, Liu H, Xu T, Zheng W, Fan P, Li H, Wu X, Zhu X, Duan X and Hu W 2017 *ACS Nano* **11** 4892
[60] Chen J, Bai Y, Qi M, Zhang W, Qin C, Fan X and Xiao L 2025 *Adv. Mater.* **37** 2415214
[61] Lu X, Xie B, Yang Y, Zhang Y, Kong X, Li J, Ding F, Wang Z J and Liu J 2024 *Phys. Rev. Lett.* **132** 056601
[62] Staley N E, Wu J, Eklund P, Liu Y, Li L and Xu Z 2009 *Phys. Rev. B* **80** 184505
[63] Ozaki T 2003 *Phys. Rev. B* **67** 155108
[64] Ozaki T and Kino H 2004 *Phys. Rev. B* **69** 195113
[65] Grimme S, Antony J, Ehrlich S and Krieg H 2010 *J. Chem. Phys.* **132** 154104
[66] Michaud-Rioux V, Zhang L and Guo H 2016 *J. Comput. Phys.* **307** 593
[67] Kresse G and Hafner J 1993 *Phys. Rev. B* **47** 558
[68] Kresse G and Hafner J 1994 *Phys. Rev. B* **49** 14251
[69] Kresse G and Furthmüller J 1996 *Phys. Rev. B* **54** 11169
[70] Kresse G and Joubert D 1999 *Phys. Rev. B* **59** 1758
[71] Moon P and Koshino M 2012 *Phys. Rev. B* **85** 195458
[72] Mele E J 2010 *Phys. Rev. B* **81** 161405
[73] Cheung C T S, Goodwin Z A H, Han Y, Lu J, Mostofi A A and Lischner J 2024 *Nano Lett.* **24** 12088
[74] Guinea F and Walet N R 2019 *Phys. Rev. B* **99** 205134
[75] Miao W, Li C, Han X, Pan D and Dai X 2023 *Phys. Rev. B* **107** 064501
[76] Uchida K, Furuya S, Iwata J I and Oshiyama A 2014 *Phys. Rev. B* **90** 155451
[77] Xie B and Liu J 2023 *Phys. Rev. B* **108** 094115
[78] Wickramaratne D, Khmelevskyi S, Agterberg D F and Mazin I I 2020 *Phys. Rev. X* **10** 041003
[79] Enaldiev V, Zólyomi V, Yelgel C, Magorrian S and Fal'ko V I 2020 *Phys. Rev. Lett.* **124** 206101
[80] Kim H, Choi Y, Lantagne-Hurtubise É, Lewandowski C, Thomson A, Kong L, Zhou H, Baum E, Zhang Y, Holleis L, Watanabe K, Taniguchi T, Young A F, Alicea J and Nadj-Perge S 2023 *Nature* **623** 942
[81] Shen C, Ledwith P J, Watanabe K, Taniguchi T, Khalaf E, Vishwanath A and Efetov D K 2023 *Nat. Mater.* **22** 316
[82] Christos M, Sachdev S and Scheurer M S 2022 *Phys. Rev. X* **12** 021018
[83] Han Z, Herzog-Arbeitman J, Bernevig B A and Kivelson S A 2024 *Phys. Rev. X* **14** 041004
[84] Gani Y S, Steinberg H and Rossi E 2019 *Phys. Rev. B* **99** 235405
[85] Xie Y M and Law K T 2023 *Phys. Rev. Lett.* **131** 016001
[86] Qin W and MacDonald A H 2021 *Phys. Rev. Lett.* **127** 097001